Systematic Characterization of Degas-driven Flow for PDMS Microfluidic Devices

David Y. Liang[1], Augusto M. Tentori[1], Ivan K. Dimov[1,2], and Luke P. Lee[,1]*

1. Biomolecular Nanotechnology Center, Berkeley Sensor and Actuator Center, Department of Bioengineering, University of California, Berkeley, USA.

2. Department of Biomedical Engineering, Universidad de Valparaíso, Valparaíso, Chile

* to whom correspondence should be addressed at:

E-mail: lplee@berkeley.edu Phone : +1 510 666 3352 Fax : +1 510 642-5835

ABSTRACT

Degas-driven flow is a novel phenomena used to propel fluids in poly(dimethylsiloxane) (PDMS)-based microfluidic devices without requiring any external power. This method takes advantage of the inherently high porosity and air solubility of PDMS by removing air molecules from the bulk PDMS before initiating the flow. The dynamics of degas-driven flow are dependent on channel and device geometries and are highly sensitive to temporal parameters. These dependencies have not been fully characterized, hindering broad use of degas-driven flow as a microfluidic pumping mechanism. Here, we characterize, for the first time, the effect of various parameters on the dynamics of degas-driven flow, including channel geometry, PDMS thickness, PDMS exposure area, vacuum degassing time, and idle time at atmospheric pressure before loading. We investigate the effect of these parameters on flow velocity as well as channel fill time for the degas-driven flow process. Using our devices, we achieved reproducible flow with a standard

deviation of less than 8% for flow velocity, as well as maximum flow rates of up to 3 nL/sec and mean flow rates of approximately 1-1.5 nL/sec. Parameters such as channel surface area and PDMS chip exposure area were found to have negligible impact on degas-driven flow dynamics, whereas channel cross-sectional area, degas time, PDMS thickness, and idle time were found to have a larger impact. In addition, we develop a physical model that can predict mean flow velocities within 6% of experimental values and can be used as a tool for future design of PDMS-based microfluidic devices that utilize degas-driven flow.

MANUSCRIPT

Introduction

Over the past decade, many methods have been developed in the area of fluid pumping for PDMS-based microfluidic devices.[1] The two most common methods include pressure-driven and electrokinetic-driven pumping. Pressure-driven pumping can be achieved by either positive or negative pressure, which push or pull fluids through microfluidic systems. However, pressure-driven pumping relies on equipment such as syringe pumps, which are bulky and expensive, and can cause mechanical bulging of PDMS microchannels during the channel filling process.[2] Electrokinetic-driven pumping, on the other hand, utilizes electroosmotic flow, which implements integrated electrodes that generate the electric fields necessary for fluid movement. However, the drawbacks of electrokinetic-driven pumping include buffer incompatibility and frequent changes to voltage settings,[3] as well as undesired consequences such as heating and bubble formation.[4] Although pressure-driven and electrokinetic pumping are commonly used to supply samples and reagents to microfluidic devices, they both require external power sources, which may be undesirable in applications such as point-of-care diagnostics in developing nations.

Recently, many developments have been made to enable power-free microfluidic pumping, such as droplet-based passive pumping,[5] evaporation,[6,7] capillary flow,[8] and gravity-driven flow.[9,10] Droplet-based passive pumping[5] and evaporation[6,7] systems are very simple to operate and set up, but are limited by the fact that they require device pre-priming and ambient temperature and humidity control - otherwise, the pumping is not reproducible. Passive fluid propulsion using capillary action/surface tension[8] requires hydrophilic surfaces for aqueous solutions (e.g. lateral flow assays, which require multi-membrane constructs). This increases the manufacturing complexity if glass substrates must be used or adds additional manufacturing steps for producing hydrophilic coatings on hydrophobic substrates. Gravity-driven flow[9,10] is another passive flow mechanism that is simple to set up, but it requires initial device priming and external tubing for generating a gravity-based pressure head, which limits the system miniaturization.

A simpler approach that does not require hydrophilic surface coatings or humidity/temperature controls and can be directly integrated at the micro-scale is degas-driven flow in porous material microfluidics, such as poly(dimethylsiloxane) (PDMS) microfluidics. The degas-driven flow mechanism takes advantage of the inherent porosity and air solubility of PDMS. By vacuuming air from the bulk PDMS, a pressure difference relative to atmospheric pressure is created. After a sample is loaded onto closed microchannels, this pressure difference causes air inside the microchannels to diffuse into the bulk PDMS. As air diffuses from the channels into the PDMS, the pressure drop relative to atmospheric pressure inside the channels pulls fluids from inlets into the microfluidic device. Thus, devices that utilize this phenomenon are capable of running without any external power. Fig. 1 shows a basic schematic illustrating this mechanism. This power-free pumping has previously been demonstrated for microchip immunoassays,[11,12,13,] gold nanoparticle-based DNA analysis,[14,15,16] and cell loading.[17]

To the best of our knowledge, only one simple model for describing the dynamics of degas-driven flow has been proposed,[14] but this model fails to include several physical aspects of degas-driven flow that affect flow properties. The model proposes that the liquid flow rate is proportional to the rate of air diffusion from the channels to the bulk PDMS and the inner channel surface area. The model does not include parameters for channel fluidic resistance and does not account for the fact that liquid-free inner channel volume and surface area decrease as liquid fills the channels. As a result the model can only produce rough order of magnitude estimations and is not able to predict the flow rates generated by degas driven flow. Acquiring a more detailed understanding of degas-driven flow through experimental characterization and the development of a more accurate physical model will assist in the application of this pumping mechanism to a broader range of microfluidic applications.

Here, we investigate the effect of various parameters on degas-driven flow, including channel geometry, channel surface area, PDMS thickness, PDMS exposure area, vacuum degas time, and post-vacuum idle time that the device is exposed to atmospheric conditions before sample loading. Specifically, we measure flow velocity and channel fill time for each parameter in order to characterize the kinetics of the degas-

driven flow process. Our experimental procedure is outlined in Supplemental Material, Fig. 1. In addition, we develop a physical model that shows a high consistency with our experimental data, which can be used as a tool for future design of PDMS microfluidic devices that implement degas-driven flow.

EXPERIMENTAL

Microfluidic devices

Several microfluidic devices of different geometries, as shown in Supplemental Material, Fig. 2, were fabricated to test the effects of various device and experiment parameters on the kinetics of degas-driven flow. All microfluidic devices used in the experiments were designed using 50 μm high dead-end channels with a single 1 mm diameter inlet for each channel. We initially started with bonded devices, but we did not see a difference in results between bonded and unbonded devices and proceeded with unbonded devices to increase the number of experiments we could do.

To characterize the effect of channel surface area, we designed a device with straight channels ending in varying fork-like dead-end structures (Supplemental Material, Fig. 4) in order to maintain a constant volume with variable surface area (ranging from 8.40 mm^2 to 16.00 mm^2) as shown in Fig. 2A. The straight channels were 35 mm long and 50 μm wide. The 4.1 mm thick PDMS device was degassed for 2 hours, and samples were loaded 2 minutes after the device was exposed to atmospheric conditions. A similar device with thickness 2.2 mm and degas time 2 hours was used to characterize the reproducibility of degas-driven flow.

To characterize the effect of channel cross-sectional area, we designed a device with straight channels with lengths of 35 mm and widths that varied from 50 μm to 500 μm, as shown in Fig. 3A. The 2.2 mm thick device was degassed for 2 hr with an idle time of 2 min.

To characterize the effect of PDMS exposure area, we compared the two practical extremes of PDMS exposure area (55% and 5%) using the channel with 8.85 mm^2 surface area in Fig. 2A. A PDMS exposure area of 55% was achieved by placing the PDMS device on top of a glass slide, the traditional setup for

most PDMS microfluidic devices. A PDMS exposure area of 5% was achieved by sandwiching the PDMS device between two glass slides and immersing the device in silicone oil, leaving only the inlet region open to ambient air. The 2.2 mm thick device was degassed for a minimum 3 hours with an idle time of 2 min for both exposure areas.

To characterize the effect of PDMS thickness, the channel with 8.85 mm^2 surface area in Fig. 2A was used, and the thickness was varied between 0.9 mm and 10.2 mm. The device was degassed for 2 hours with an idle time of 2 min for all thicknesses.

To characterize the effect of degas time, the channel with 8.85 mm^2 surface area in Fig. 2A was used. The 4.1 mm thick device was held at an idle time of 2 min for all degas times. To characterize the effect of idle time, the channel with 8.85 mm^2 surface area in Fig. 2A was used. The 2.2 mm thick device was degassed for 2 hr for all idle times.

To characterize the feasibility of our physical model, we compared the max and mean velocities of our model to our experimental data for a device with varying S-curve channel lengths ranging from 25 mm to 65 mm. The 4.1 mm thick device was degassed for 24 hours with an idle time of 2 min. We also compared the max and mean velocities of our model to our experimental data for a device with varying cross-sectional areas, as shown in Fig. 3A. The 2.2 mm thick device was degassed for 24 hours with an idle time of 2 min.

A table summarizing the device and experiment parameters for each figure is shown below:

	Figure #				
	2B) Channel surface area	**2C) Reproducibility**	**3B) Channel cross-sectional area**	**4B) PDMS exposure area**	**5B) Degas time**
Degas time	24 hr	2 hr	2 hr	3 hr	Variable (10 min to 24 hr)
Idle time	2 min	2 min	2 min	2 min	2 min
PDMS thickness	4.1 mm	2.2 mm	2.2 mm	2.2 mm	4.1 mm
PDMS exposure area	55%	55%	55%	Variable (55% and 5%)	55%
Surface area	Variable (8.40 to 16.00 mm^2)	Variable (8.40 to 16.00 mm^2)	Variable (0.005 to 7.005 mm^2)	8.85 mm^2	8.85 mm^2
Length	35 mm	35 mm	35 mm	35 mm	35 mm
Width	50 µm	50 µm	Variable (50 to 500 µm)	50 µm	50 µm
Height	50 µm	50 µm	50 µm	50 µm	50 µm

	Figure #				
	6B) PDMS thickness	**7B) Idle time**	**8A) Model: Channel Length, 2 min Idle Time**	**8B) Model: Channel Length, 10 min Idle Time**	**8C) Model: Channel Cross-sectional Area**
Degas time	2 hr	2 hr	24 hr	24 hr	24 hr
Idle time	2 min	Variable (2 to 10 min)	2 min	10 min	2 min
PDMS thickness	Variable (0.9 to 10.2 mm)	2.2 mm	4.1 mm	4.1 mm	2.2 mm
PDMS exposure area	55%	55%	55%	55%	55%
Surface area	16.00 mm^2	8.85 mm^2	Variable (5.005 to 13.005 mm^2)	Variable (5.005 to 13.005 mm^2)	Variable (0.005 to 7.005 mm^2)
Length	35 mm	35 mm	Variable (25 to 65 mm)	Variable (25 to 65 mm)	35 mm
Width	50 µm	50 µm	50 µm	50 µm	Variable (50 to 500 µm)
Height	50 µm	50 µm	50 µm	50 µm	50 µm

Table 1: Summary of all experiment and device parameters, including degas time, idle time, PDMS thickness, PDMS exposure area, surface area, length, width, and height of the PDMS microchannels.

5 Device fabrication

The microfluidic channels were fabricated using standard soft lithography replica molding techniques. A single-layer mold was created using negative photoresist, SU8-2050 (Microchem, USA), which was spun onto a clean silicon wafer using a spinner (P6700 Specialty Coating Systems, Inc., USA). The resist (5 mL) was spread onto the wafer at 500 rpm for 10 s and then ramped up at an acceleration of 300 rpm/s

to 3,000 rpm, at which rate the sample was spun for 30 s to form a 50 μm layer. The wafer was then soft baked at 65 ºC for 3 min and 95 ºC for 15 min, then UV-exposed for 10 s at 10 mW/cm^2 using a Karl-Suss KSM MJB-55W mask aligner. The wafer was then post-exposure baked for 2 min at 65 ºC and 10 min at 95 ºC, allowed to cool to room temperature, developed in Microposit EC Solvent (Chestech, Ltd., UK) developer for 10 min, and finally blown dry with nitrogen. PDMS (Sylgard 184, Dow Corning) was prepared according to the instructions of the manufacturer, degassed in a vacuum chamber for 30 min, then poured onto the SU8 mold and cured at room temperature for 48 hours. The PDMS was then peeled off the mold, and the individual devices were cut out using a single-edge razor blade. Fluid inlets were punched with a 1 mm outer diameter flat-tip needle for tube connections. The devices were then placed directly onto 25 x 50 x 0.4 mm glass cover slides (VWR International Inc., USA) and manually pressed together to form reversible seals. The surfaces of the PDMS devices were cleaned using Scotch tape before degassing.

Flow characterization

All devices were degassed in a vacuum chamber at ~100 mTorr for a minimum 2 hours before testing such that all the air that could be removed from the devices was removed, with the exception of some devices specifically degassed for shorter periods to investigate the effect of degas time on degas-driven flow. The devices were then pulled out of the vacuum chamber and placed under an optical microscope. Drops of blue food coloring dye (McCormick) were then placed directly on top of each inlet using a micropipette. The idle time, the amount of time in ambient air before fluid was added to the inlets, was recorded for all devices. A mounted Nikon digital camera was used to acquire time-lapse images of the microfluidic channels until they were completely filled with dye, and QCapture Pro 6.0 software was used for image recording.

Data analysis

The acquired time-lapse images were analyzed using a MATLAB script to count the number of pixels in each video frame corresponding to the food coloring dye. The numbers of pixels were then converted to

fluid volumes, and the data was analyzed to calculate flow velocities during the degas-driven flow process. Unless otherwise specified, data shown accounts for the last 10.7 mm of the microchannel length, as the field of view of the microscope objective used was unable to capture the entire microchannel, and all curves are offset to the origin in order to compare individual data curves. Experimental data obtained from the microfluidic device was compared to the physical model that was numerically solved using the MATLAB v.9 ode15s solver. The governing equations and derivation of the physical model is described in the Supplemental Material.

RESULTS

Channel surface area

To investigate whether channel surface area can be modified with the aim of achieving specific flow rates, we measured the fluid volume and flow velocity profiles of channels with dead-end geometries of varying surface areas: 8.40, 8.85, 10.02, 12.01, and 16.00 mm^2, as shown in Fig. 2A. We varied surface area while maintaining channel volume constant. Standard soft lithography fabrication methods limit the width-to-height aspect ratio of our device features to 2:1. With this fabrication limitation in mind, we were able to vary the surface area by almost a factor of 2 while maintaining constant volume. The flow velocity and fluid volume profiles were observed to be similar for all surface areas, as shown in Fig. 2B. We also observed that the inter-channel proximity does affect the degas-driven flow. More details are provided in Supplemental Material, Fig. 4.

Reproducibility

A single PDMS device with channels of varying surface areas was tested five times to demonstrate reproducibility of the degas-driven flow process. Between each test, the device was cleaned with IPA and DI water, then dried using nitrogen gas and degassed for two hours. The mean flow velocities were calculated to be the following: 1.176 nL/sec for 16.00 mm^2, 1.019 for 12.01 mm^2, 1.046 for 10.02 mm^2, and 0.859 for 8.85 mm^2. As a conservative estimate of our measurement uncertainty, we selected the

largest standard deviation obtained from the four channels, which was 7.59% for flow velocity and 11.49% for fluid volume. We define our uncertainty range as ±1.96σ, which should include 95% of our distribution, assuming it is normal. These two measures of uncertainty were used as the error bars for all data plots. Our results, as shown in Fig. 2C, demonstrate that degas-driven flow can reproducibly load samples with consistent flow velocities, which is an important criterion for many microfluidic-based applications in which precise control of flow velocity is necessary.

Channel cross-sectional area

Since channel cross-sectional area is a key parameter that affects flow rates within a microfluidic system, its effect was investigated by measuring the fluid volume and flow velocity profiles using devices with straight dead-end channels of varying widths: 50, 100, 200, 350, and 500 μm, as shown in Fig. 3A. As expected, the amount of time required for the channels to fill was found to increase as channel width increased (Fig. 3B), since the total volume of the channel increases as channel cross-sectional area increases. The flow velocity was found to increase as the channel cross-sectional area increased, and the flow velocity was found to decay at a similar rate for all five widths. By altering the microchannel cross-sectional area from 2,500 to 25,000 μm^2, we are able to generate maximum flow velocities ranging from 0.92 and 2.57 nL/sec, respectively, nearly a 3-fold difference.

PDMS chip exposure area

Since we hypothesize that the degas-driven flow is caused by the diffusion of air from the atmosphere into the bulk PDMS, we investigated the effect of the overall PDMS exposure area, the amount of PDMS surface area exposed to ambient air, on the degas-driven flow kinetics. Two amounts of PDMS exposure area, ~55% and ~5% exposure, were tested (Fig. 4A). Based on our results as shown in Fig. 4B, the differences in PDMS exposure area did not appear to affect flow velocity, which initially peaked at approximately 1.5 nL/sec and gradually decayed at a rate of approximately 0.06 nL/sec^2. Thus, we believe that PDMS exposure area does not considerably impact degas-driven flow dynamics.

Degas time

Since degas time affects the amount of air that is degassed from the bulk PDMS and thus the pressure difference between the PDMS and the atmosphere, the effect of degas time was investigated by degassing the microfluidic devices for varying lengths of time: 10, 45, 120, and 1440 min, as shown in Fig. 5A. Although flow velocities with a degas time of 45, 120, and 1,440 min were comparable, with values between 1 to 1.5 nL/sec, flow velocities with a degas time of 10 min were considerably smaller with values of approximately 0.25 to 0.5 nL/sec (Fig. 5B). With shorter degas times, we hypothesize that less air is degassed from the bulk PDMS, resulting in a smaller pressure difference that causes the fluid to be pulled less quickly into the channels. However, since additional degas time past 45 min did not make a large impact on flow velocity, a maximum degas time threshold near 45 min most likely exists, beyond which the bulk PDMS is entirely degassed and will have a reproducible flow velocity profile.

PDMS thickness

We investigated the effect of PDMS thickness by fabricating devices with thicknesses of 0.9, 2.2, 4.1, and 10.2 mm, as shown in Fig. 6A. The flow velocities for the 2.2, 4.1, and 10.2 mm thick devices were comparable with a maximum velocity of about 1.5 nL/sec (Fig. 6B). However, the PDMS device with a thickness of 0.9 mm had considerably slower fluid flow with a maximum velocity of about 0.5 nL/sec. The device also took considerably longer to fill, approximately 60 sec as opposed to 20 sec as seen in the thicker PDMS devices. Thus, by decreasing the PDMS thickness of our device from 2.2 to 0.9 mm, we observed a three-fold decrease in maximum flow velocity and a three-fold increase in channel filling time. In addition, although the 16.00 mm^2 channel resulted in flow, the other three channels resulted in no flow (Supplemental Material, Fig. 5), which shows that a minimum PDMS thickness between 0.9 and 2.2 mm is required for degas-driven flow to occur when the device is degassed for at least 2 hours with an idle time of 2 min.

Idle time

Like degas time, the idle time affects the amount of air present in the bulk PDMS during fluid loading and thus the pressure difference that drives the degas-driven flow. The effect of idle time was investigated

by leaving the microfluidic devices out in ambient air for varying lengths of time after degassing: 2, 4, 7, and 10 min, as shown in Fig. 7A. The velocities for the longest idle time, 10 min, were found to be slightly smaller, peaking initially at approximately 1.25 nL/sec as opposed to 1.75 nL/sec as seen in the other three idle times (Fig. 7B). This suggests that idle times of up to 7 min do not considerably affect the flow dynamics for channels with additional end surface area, meaning that users can load samples into the microfluidic device within 7 min of exposing the device to atmospheric pressure without changing the flow profile. For the device with varying cross-sectional areas, as shown in Fig. 3A, an idle time of 10 min resulted in some channels not filling completely (Supplemental Material, Fig. 6). We hypothesize that with longer idle times, more ambient air diffuses back into the bulk PDMS, resulting in a smaller pressure difference that causes the fluid to be pulled less quickly into the channels.

Physical model of degas-driven flow

To be able to design microfluidic devices that use this degas-driven flow mechanism, it is important to understand the dominating physical phenomena and the relevant geometrical parameters. For this reason, we developed a physical model that takes into account the principal components that govern degas-driven flow within a microfluidic system, which can predict the system dynamics observed in the data and, more importantly, be used as a tool for future design. We hypothesize that the principal physical phenomena that drive degas-driven flow are the diffusion of air through the walls of the microchannel into the bulk PDMS and pressure-driven Pousille-like fluid flow within microchannels.

The surface area of exposed fluid is nearly 3 orders of magnitude (approximately 0.0025 mm^2 compared to 2.14 mm^2) smaller than the total surface area of the empty PDMS channel, calculated at the point 10.7 mm before the end of the straight channel where data collection begins for the surface area devices. In addition, the gas diffusion rate is considerably smaller than the fluid flow rate. Therefore, we believe the effect of gas diffusion through the infiltrating liquid is negligible compared to the flux of air through the PDMS. As air diffuses from the microchannel into the degassed PDMS, a pressure difference develops inside the microchannel relative to the external atmospheric pressure. This pressure difference drives the

flow. As the microchannel fills with fluid, both the surface area through which the air can diffuse into the PDMS and the free microchannel volume decrease. Both of these effects, as well as the increasing air concentration in the PDMS, affect the rate at which air diffuses from the microchannel into the PDMS, and thus the air pressure inside the microchannel.

The Supplemental Material shows the derivation of the governing equations that were numerically solved to calculate the fluid flow velocity. We used our physical model to calculate the degas-driven flow dynamics for microchannels of varying lengths at different idle times (Fig. 8A and 8B) and varying cross-sectional areas (Fig. 8C). The effect of the fork-like dead end structures present in some of the devices is not easily accountable in our model, which assumes a straight channel for its estimation of fluidic resistance. For this reason, we chose to compare the results from our theoretical model to the data obtained from channels of varying cross-sectional areas and the S-curve channels of varying lengths with no fork-like dead end structures. Model parameters were obtained from literature[18], experimental conditions, or empirically, as mentioned in the Supplemental Material section titled “Physical Model." The two parameters obtained empirically (referred to as K1 and K2) were estimated from one set of data, and then those same values were used for the rest of our comparisons to demonstrate the predictive value of our model (described in more detail in the Supplemental Material).

For the S-curves of varying lengths with 2 min idle time (Fig. 8A), our model predicts, on average, maximum velocity values within approximately 16% and mean velocity values within approximately 9% of experimental values. For the S-curves of varying lengths with 10 min idle time (Fig. 8B), our model predicts, on average, maximum velocity values within approximately 10% and mean velocity values within approximately 9% of experimental values. For the channels of varying cross-sectional areas with 2 min idle time (Fig. 8C), our model predicts, on average, maximum velocity values within approximately 40% and mean velocity values within approximately 2% of experimental values. A direct comparison between our experimental data and our theoretical model can be seen in Supplemental Material, Fig. 3.

These results support the use of our physical model as a tool to predict degas-driven flow behavior in PDMS microfluidic devices.

DISCUSSION

Our findings show that the degas-driven flow phenomena is highly reproducible and is capable of generating maximum flow rates of up to 3 nL/sec, with a mean peak flow rate of approximately 1-1.5 nL/sec. Channel surface area (with constant volume) and PDMS chip exposure area were found to have a minimal impact on degas-driven flow dynamics, whereas channel cross-sectional area, degas time, PDMS thickness, and idle time were found to have a larger impact. Varying cross-sectional area leads to both decreased fluidic resistance and increased surface area. Because varying surface area did not lead to large differences in observed flow rates, we believe that the faster flow rates observed in channels with larger cross-sectional areas are primarily due to decreased channel fluidic resistance.

From the data obtained from our devices with varying cross-sectional area, by not having fork-like structures, we see a clean exponential decay. In an effort to generate a more constant flow rate, as compared to the native exponential decay, we included a fork-like dead end structure that increases the channel surface area. We measure the effects of the PDMS exposure area, degas time, PDMS thickness, and idle time in combination with the fork-like dead end structure. Adding the fork-like structure reduces the exponential decay and makes the flow velocity less variable for a given length.

Short degas times were observed to lead to decreased flow rates. For our device dimensions, a degas time of 45 min was sufficient to achieve the maximum degassing in the PDMS, and degassing for longer than 45 min did not lead to a faster flow rate. Varying PDMS thickness did lead to variations in flow rates. For 2 min idle times, a minimum thickness >0.9mm was necessary to obtain flow. As expected, increased idle times led to slower flow rates. Interestingly, having extra surface area structures at the ends of channels did mitigate the effect of increased idle times compared to simple dead-end channels. Designing devices that can operate with the same performance for a range of idle times is important given the

unavoidable user variations that will occur in a real-world setting. Our results indicate that device design can be optimized to lead to more robust performance for different idle times.

The theoretical model can be used to obtain estimates of flow rate ranges that can be achieved using specific device resistances and experiment parameters. The model shows good predictive value for the channels of different lengths at different idle times and channels with varying cross-sectional area. For the S-curves of varying lengths, our model predicts, on average, maximum velocity values within approximately 13% and mean velocity values within approximately 9% of experimental values. For the channels of different lengths, we were able to collect data for the entire length of the channel, given that the S-curve design of our channels fit in the microscope's field of view. The downside, however, is that we do not expect winding channels to behave exactly the same as straight channels, given the close proximity between different channel sections (see Supplemental Material, Fig. 4). This effect might explain some of the discrepancies between experimental and theoretical results. For the channels of varying cross-sectional area, our model predicts, on average, maximum velocity values within approximately 40% and mean velocity values within approximately 2% of experimental values. Data was collected from the last 10.7 mm of the channels and not the entire channel. The measured maximum and mean velocities calculated correspond to this section of the channels only. We believe that this might explain the larger discrepancy in maximum velocity measured and predicted by our model, given that we are not able to compare to the velocity along the entire channel.

CONCLUSION

We characterize the degas-driven flow phenomenon for PDMS microfluidic devices by investigating the effects of various parameters on fluid flow velocity and channel filling time. These parameters included both device parameters (channel cross-sectional area, channel surface area, PDMS thickness, and PDMS exposure area) as well as experiment parameters (degas time and post-vacuum idle time). We demonstrate that these parameters can be modulated to meet the desired degas-driven flow kinetics for a given

application. By characterizing the device and experimental parameters, it is possible to fabricate microfluidic devices with precise geometries and specify minimum device parameter thresholds under which the flow velocity can be expected to behave in a reproducible manner.

Specifically, we saw that for 4.1 mm thick microfluidic devices with a channel width and height of 50 microns, a degas time of approximately 45 min was sufficient for complete degassing. For 2.5 mm thick devices, an idle time of approximately 7 min was still capable of producing stable flow, given that the devices were completely degassed beforehand. This is an important result as it illustrates that device design can be optimized to reduce the variabilities created by user intervention and idle time before loading.

Using the devices mentioned earlier, we were able to obtain maximum flow velocities ranging from approximately 0.2 to 3 nL/sec, depending on which device geometry was used. Both surface area and PDMS exposure area were found to have negligible effects on the fluid flow velocity, as did PDMS thickness down to 2.2 mm, assuming complete degassing in all cases. We were able to obtain reproducible flow with a standard deviation of less than 8% for flow velocity. The flow kinetics can be estimated using the physical model derived here, which can predict, on average, mean velocity values within approximately 6% and maximum velocity values within 22% of the empirical values for PDMS devices of different geometries used under different conditions.

This flow kinetics data can help to optimize sample loading and testing specifications for numerous applications involving PDMS-based lab-on-a-chip devices. The flow velocity profiles from these devices can be used to estimate similar degas-driven flow profiles in other systems. In addition, the derived physical model can be adapted to other designs and conditions to observe how the degas-driven flow system is affected by specific parameters. Characterization of these parameters will undoubtedly help users design future microfluidic devices, as well as help expand the range of possible applications for PDMS-based degas-driven flow.

ACKNOWLEDGEMENTS

This research was performed under an appointment to the Department of Homeland Security (DHS) Scholarship and Fellowship Program, administered by the Oak Ridge Institute for Science and Education (ORISE) through an interagency agreement between the U.S. Department of Energy (DOE) and DHS. ORISE is managed by Oak Ridge Associated Universities (ORAU) under DOE contract number DE-AC05-06OR23100. All opinions expressed in this paper are the authors' and do not necessarily reflect the policies and views of DHS, DOE, or ORAU/ORISE.

REFERENCES

[1] P. S. Dittrich, K. Tachikawa, and A. Manz. Anal. Chem. **78**, 3887-3908 (2006).

[2] M. A. Holden, S. Kumar, A. Beskok, and P. S. Cremer. J. Micromech. Microeng. **13**, 412-418 (2003).

[3] S. K. Sia and G. M. Whitesides. Electrophoresis 2003, **24**, 3563-3576 (2003).

[4] V. Studer, A. Pepin, Y. Chen, and A. Ajdari. Analyst **129**, 944-949 (2004).

[5] G. M. Walker and D. J. Beebe. Lab Chip **2**, 131-134 (2002).

[6] M. Zimmerman, S. Bentley, H. Schmid, P. Hunziker, and E. Delamarche. Lab Chip **5**, 1355-1359 (2005).

[7] N. Goedecke, J. Eijkel, and A. Manz. Lab Chip **2**, 219-223 (2002).

[8] D. Juncker, H. Schmid, U. Drechsler, H. Wolf, M. Wolf, B. Michel, N. Rooij, and E. Delamarche. Anal. Chem. **74**, 6139-6144 (2002).

[9] D. Huh, J. H. Bahng, Y. Ling, H. Wei, O. D. Kripfgans, J. B. Fowlkes, J. B. Grotberg, and S. Takayama. Anal. Chem. **79**, 1369-1376 (2007).

[10] B. Yao, G. Luo, X. Feng, W. Wang, L. Chen, and Y. Wang. Lab Chip **4**, 603-607 (2004).

[11] K. Hosokawa, M. Omata, K. Sato, and M. Maeda. Lab Chip **6**, 236-241 (2006).

[12] K. Hosokawa, M. Omata, and M. Maeda. Anal. Chem. **79**, 6000-6004 (2007).

[13] I. K. Dimov, L. Basabe-Desmonts, J. Garcia-Cordero, B. M. Ross, Y. Park, A. J. Ricco and L. P. Lee, Lab Chip, **11**, 845-850 (2011).

[14] K. Hosokawa, K. Sato, N. Ichikawa, and M. Maeda. Lab Chip **4**, 181-185 (2004).

[15] Y. Sato, K. Sato, K. Hosokawa, and M. Maeda. Anal. Biochem. **355**, 125-131 (2006).

[16] Y. Sato, K. Hosokawa, and M. Maeda. Colloids and Surfaces B: Biointerfaces, **62**, 71-76 (2008).

[17] C. Luo, X. Zhu, T. Yu, X. Luo, Q. Ouyang, H. Ji, and Y. Chen. Biotechnology and Bioengineering, **101**, 190-195 (2008).

[18] T. C. Merkel, V. I. Bondar, K. Nagai, B. D. Freeman and I. Pinnau, J. Polym. Sci. Part B, **38**, 415–434 (2000).

[19] See Supplemental material at [URL will be inserted by AIP] for a derivation of the physical model and comparisons between the physical model and experimental data.

Figure Captions

FIG 1. Photographs of vacuumed microfluidic device and enlarged schematic showing the basic physical components of degas-driven fluid flow. After the PDMS device is extracted from its vacuum-sealed container, a sample can be placed on top of the inlets of the closed microchannels at atmospheric pressure. Gas inside the microchannel diffuses into the degassed PDMS, which results in a lower pressure inside the microchannel relative to atmospheric pressure. The sample is drawn into the channels due to this pressure difference.

FIG 2. Effect of channel surface area on degas-driven flow. (A) Schematic showing device with channels of varying surface areas. Box highlights the region of the channels that the channel surface areas were calculated from. (B) Flow velocity and fluid volume profiles (inset) during channel filling for four different channel surface areas, ranging from 8.40 mm^2 to 12.01 mm^2, as indicated by the schematic. Error bars represent $\pm 1.96\sigma$ of the reproducibility measurements, and the data accounts for the last 10.7 mm of the microchannel length. (C) Reproducibility: mean flow velocities of four different channels with varying surface area using the device in (A) with a degas time of 2 hr and a thickness of 2.2 mm. Mean flow velocity was calculated as the average mean of the instantaneous velocities over the first 15 seconds, when the velocity was above 0.5 nL/sec. Error bars represent $\pm 1.96\sigma$ of the reproducibility measurements, and the data accounts for the last 10.7 mm of the microchannel length. Four of the five channels were imaged due to the 8.85 mm^2 condition being close in value to the 8.40 mm^2 condition.

FIG 3. Effect of channel cross-sectional area on degas-driven flow. (A) Schematic showing device with channels of varying widths, ranging from 50 μm to 500 μm or 0.0025 mm^2 to 0.025 mm^2 in channel cross-sectional area. (B) Polynomial fit of degree 9 (0.0025 mm^2), degree 7 (0.005 mm^2), and degree 5 (0.01 to 0.025 mm^2) to flow velocity and fluid volume profiles (inset) during channel filling for the five different channel cross-sectional areas. Raw data for fluid velocity is shown by markers. Error bars represent ±1.96σ of the reproducibility measurements, and the data accounts for the last 10.7 mm of the microchannel length.

FIG 4. Effect of PDMS exposure area on degas-driven flow. (A) Schematic showing the two conditions that were tested: 55% exposure with PDMS device placed on top of glass slide and 5% exposure with PDMS device placed between two glass slides and immersed in silicone oil. Data was obtained from the channel with surface area 8.85 mm^2 in Fig. 2A, with a thickness of 2.2 mm. (B) Flow velocity and fluid volume profiles (inset) during channel filling for the 5% and 55% PDMS exposure areas. Error bars represent ±1.96σ of the reproducibility measurements, and the data accounts for the last 10.7 mm of the microchannel length.

FIG 5. Effect of vacuum degas time on degas-driven flow. (A) Schematic showing device in vacuum chamber with varying degas times, ranging from 10 min to 24 hr. Data was obtained from the channel with surface area 8.85 mm^2 in Fig. 2A, with a thickness of 4.1 mm. (B) Flow velocity (main) and fluid volume profiles (inset) during channel filling for the four degas times. Error bars represent ±1.96σ of the reproducibility measurements, and the data accounts for the last 10.7 mm of the microchannel length.

FIG 6. Effect of PDMS thickness on degas-driven flow. (A) Schematic showing device with varying PDMS thickness, ranging from 0.9 mm to 10.2 mm. Data was obtained from the channel with surface area 16.00 mm^2 in Fig. 2A, with a degas time of 2 hr and idle time of 2 min. (B) Flow velocity and fluid volume profiles (inset) during channel filling for the four PDMS thicknesses. Error bars represent $\pm 1.96\sigma$ of the reproducibility measurements, and the data accounts for the last 10.7 mm of the microchannel length.

FIG 7. Effect of post-vacuum idle time on degas-driven flow. (A) Schematic showing device removed from vacuum chamber with varying post-vacuum idle times, ranging from 2 min to 10 min. Data was obtained from the channel with surface area 8.85 mm^2, with a thickness of 2.2 mm. (B) Flow velocity and fluid volume profiles (inset) during channel filling for the four post-vacuum idle durations. Error bars represent $\pm 1.96\sigma$ of the reproducibility measurements, and the data accounts for the last 10.7 mm of the microchannel length.

FIG 8. Effect of varying channel length, idle time, and channel cross-section on degas-driven flow. Theoretical and experimental results for maximum and mean flow velocity shown. (A) Data obtained for entire channel length for S-curve channels with lengths varying from 65 mm to 25 mm with 24 hr degas time, 2 min idle time, 4.1 mm PDMS thickness, and a 200 sec run time. (B) Data obtained for entire channel length for S-curve channels with lengths varying from 65mm to 25mm, with a 24 hr degas time, 10 min idle time, 4.1 mm PDMS thickness, and 900 sec run time. (C) Data obtained for end portion channels with cross sections varying from 0.025 mm^2 to 0.0025 mm^2, with a 24 hr degas time, 2 min idle time, 2.2 mm PDMS thickness, and a 600 sec run time. Error bars represent $\pm 1.96\sigma$ of the reproducibility measurements.

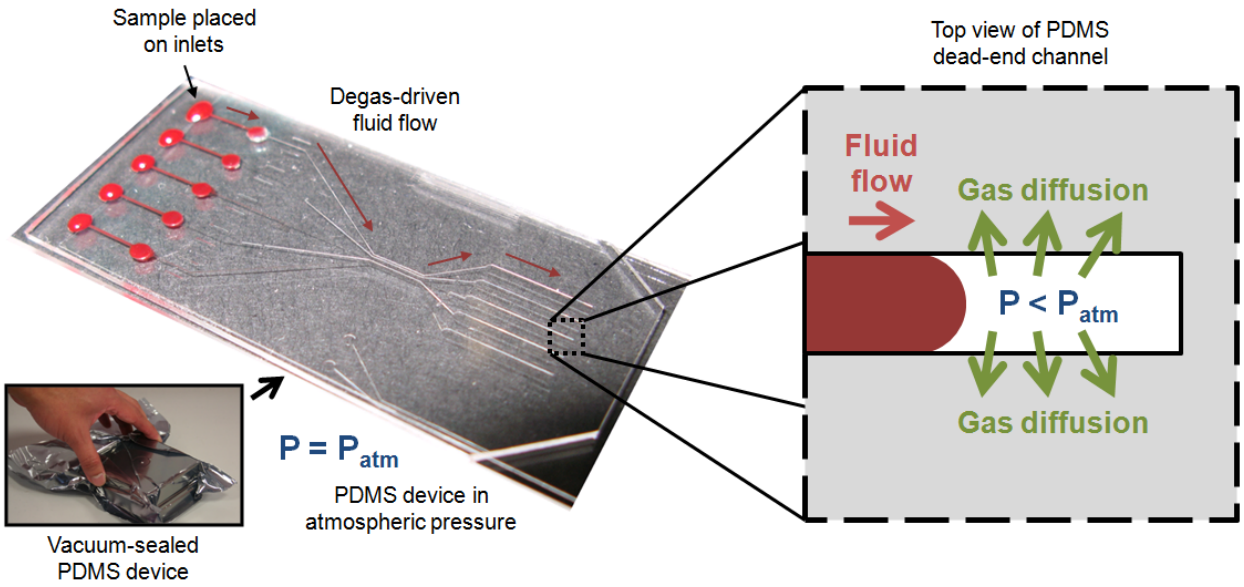

FIG 1. Photographs of vacuumed microfluidic device and enlarged schematic showing the basic physical components of degas-driven fluid flow. After the PDMS device is extracted from its vacuum-sealed container, a sample can be placed on top of the inlets of the closed microchannels at atmospheric pressure. Gas inside the microchannel diffuses into the degassed PDMS, which results in a lower pressure inside the microchannel relative to atmospheric pressure. The sample is drawn into the channels due to this pressure difference.

A

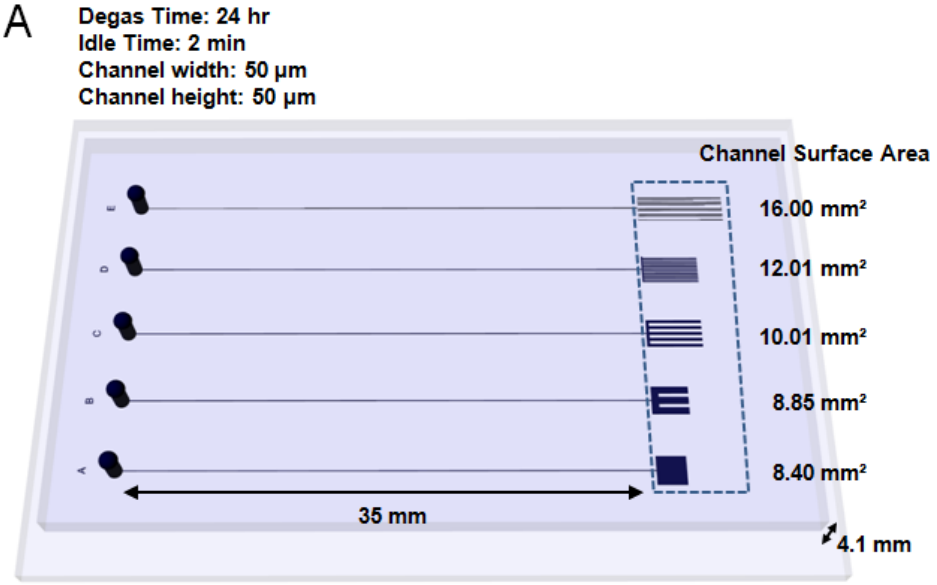
Degas Time: 24 hr
Idle Time: 2 min
Channel width: 50 µm
Channel height: 50 µm
Channel Surface Area
16.00 mm²
12.01 mm²
10.01 mm²
8.85 mm²
8.40 mm²
35 mm
4.1 mm

B

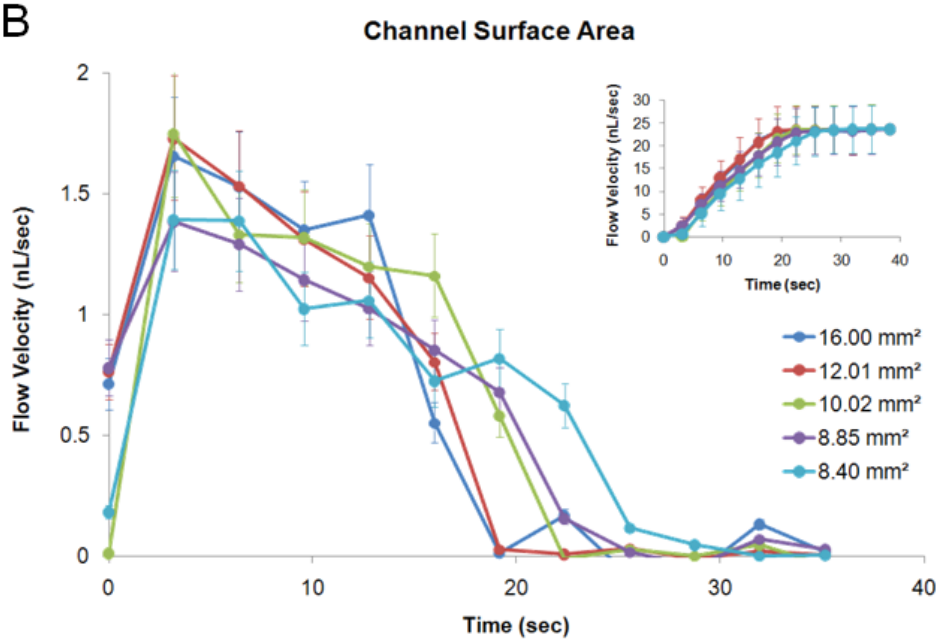
Channel Surface Area
Flow Velocity (nL/sec)
Time (sec)
16.00 mm²
12.01 mm²
10.02 mm²
8.85 mm²
8.40 mm²

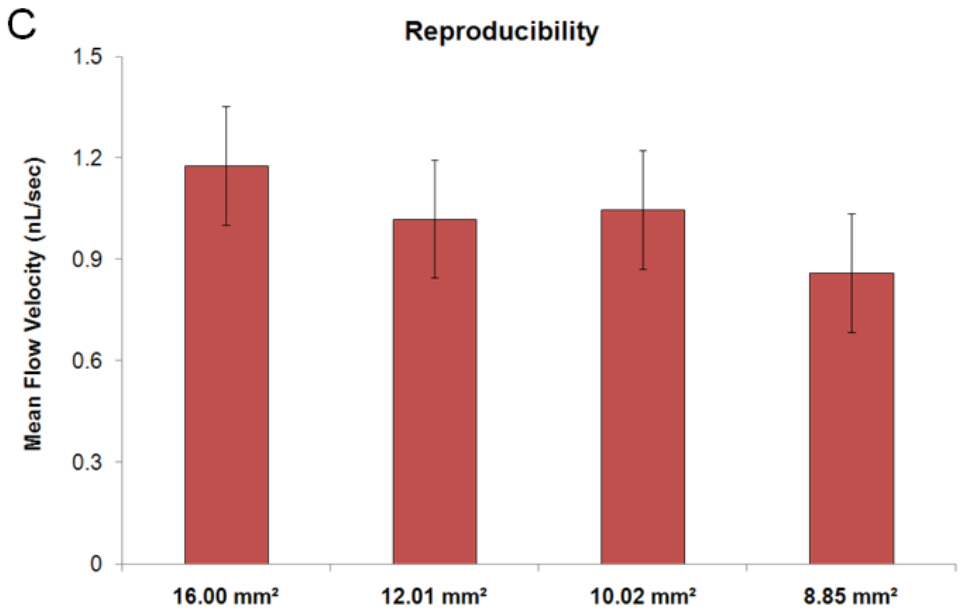

FIG 2. Effect of channel surface area on degas-driven flow. (A) Schematic showing device with channels of varying surface areas. Box highlights the region of the channels that the channel surface areas were calculated from. (B) Flow velocity and fluid volume profiles (inset) during channel filling for four different channel surface areas, ranging from 8.40 mm^2 to 12.01 mm^2, as indicated by the schematic. Error bars represent ±1.96σ of the reproducibility measurements, and the data accounts for the last 10.7 mm of the microchannel length. (C) Reproducibility: mean flow velocities of four different channels with varying surface area using the device in (A) with a degas time of 2 hr and a thickness of 2.2 mm. Mean flow velocity was calculated as the average mean of the instantaneous velocities over the first 15 seconds, when the velocity was above 0.5 nL/sec. Error bars represent ±1.96σ of the reproducibility measurements, and the data accounts for the last 10.7 mm of the microchannel length. Four of the five channels were imaged due to the 8.85 mm^2 condition being close in value to the 8.40 mm^2 condition.

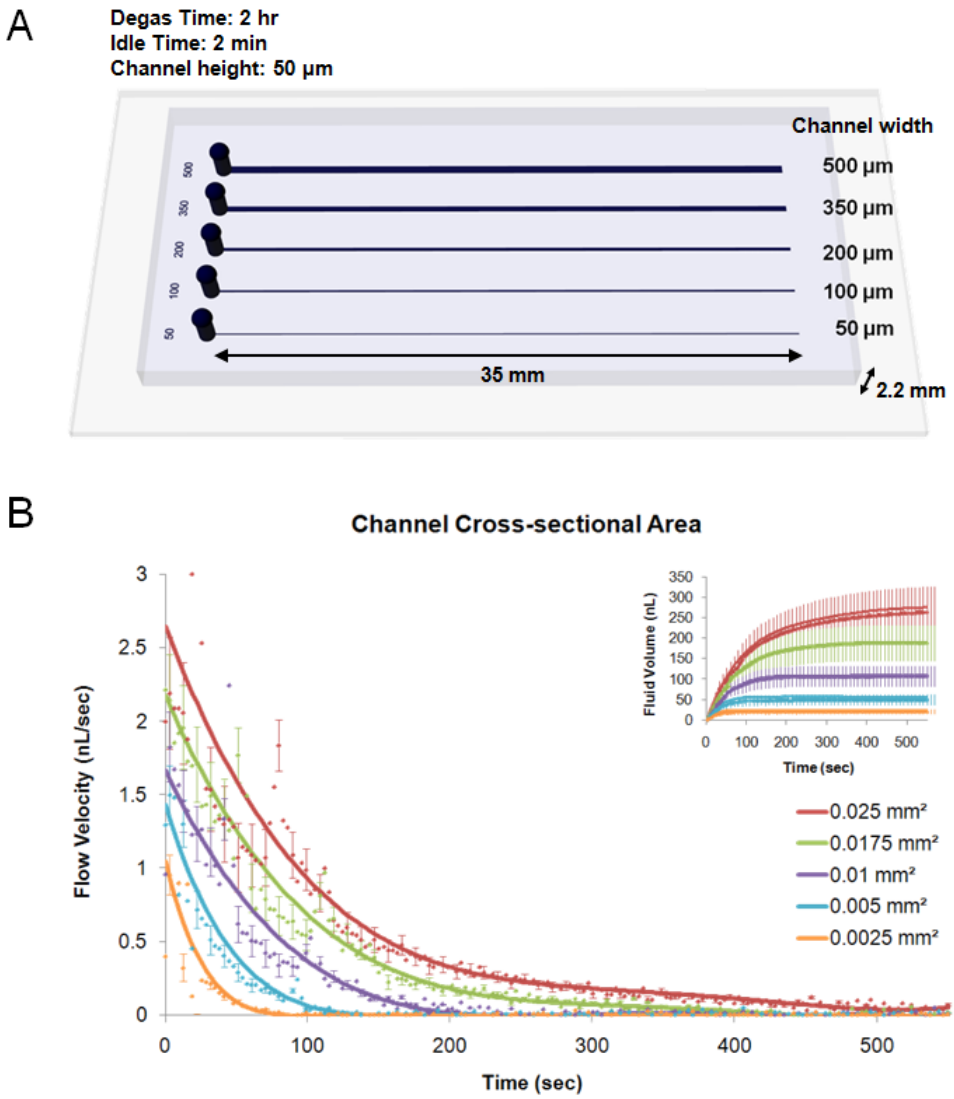

FIG 3. Effect of channel cross-sectional area on degas-driven flow. (A) Schematic showing device with channels of varying widths, ranging from 50 µm to 500 µm or 0.0025 mm^2 to 0.025 mm^2 in channel cross-sectional area. (B) Polynomial fit of degree 9 (0.0025 mm^2), degree 7 (0.005 mm^2), and degree 5 (0.01 to 0.025 mm^2) to flow velocity and fluid volume profiles (inset) during channel filling for the five different channel cross-sectional areas. Raw data for fluid velocity is shown by markers. Error bars represent ±1.96σ of the reproducibility measurements, and the data accounts for the last 10.7 mm of the microchannel length.

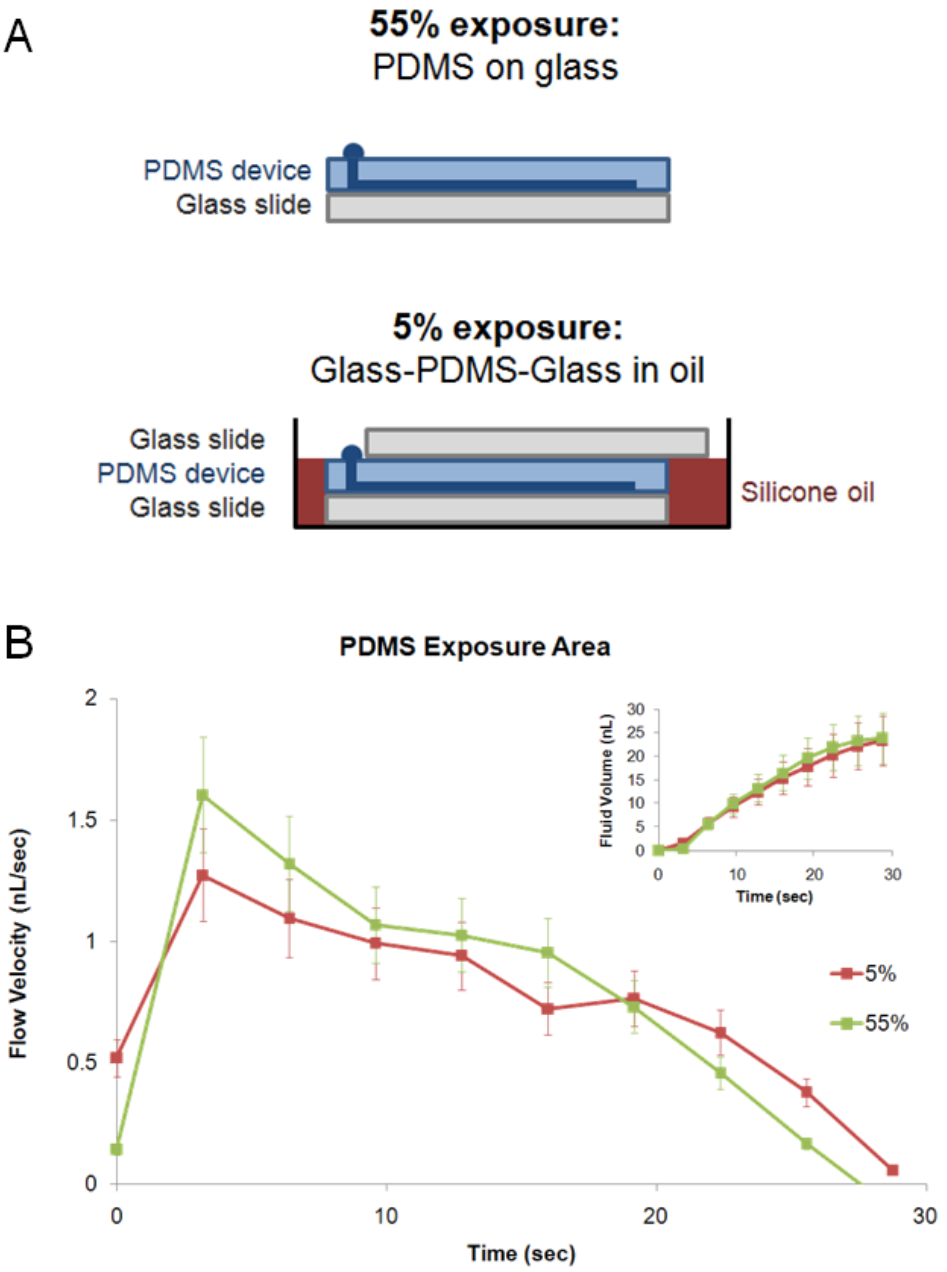

FIG 4. Effect of PDMS exposure area on degas-driven flow. (A) Schematic showing the two conditions that were tested: 55% exposure with PDMS device placed on top of glass slide and 5% exposure with PDMS device placed between two glass slides and immersed in silicone oil. Data was obtained from the channel with surface area 8.85 mm^2 in Fig. 2A, with a thickness of 2.2 mm. (B) Flow velocity and fluid volume profiles (inset) during channel filling for the 5% and

55% PDMS exposure areas. Error bars represent ±1.96σ of the reproducibility measurements, and the data accounts for the last 10.7 mm of the microchannel length.

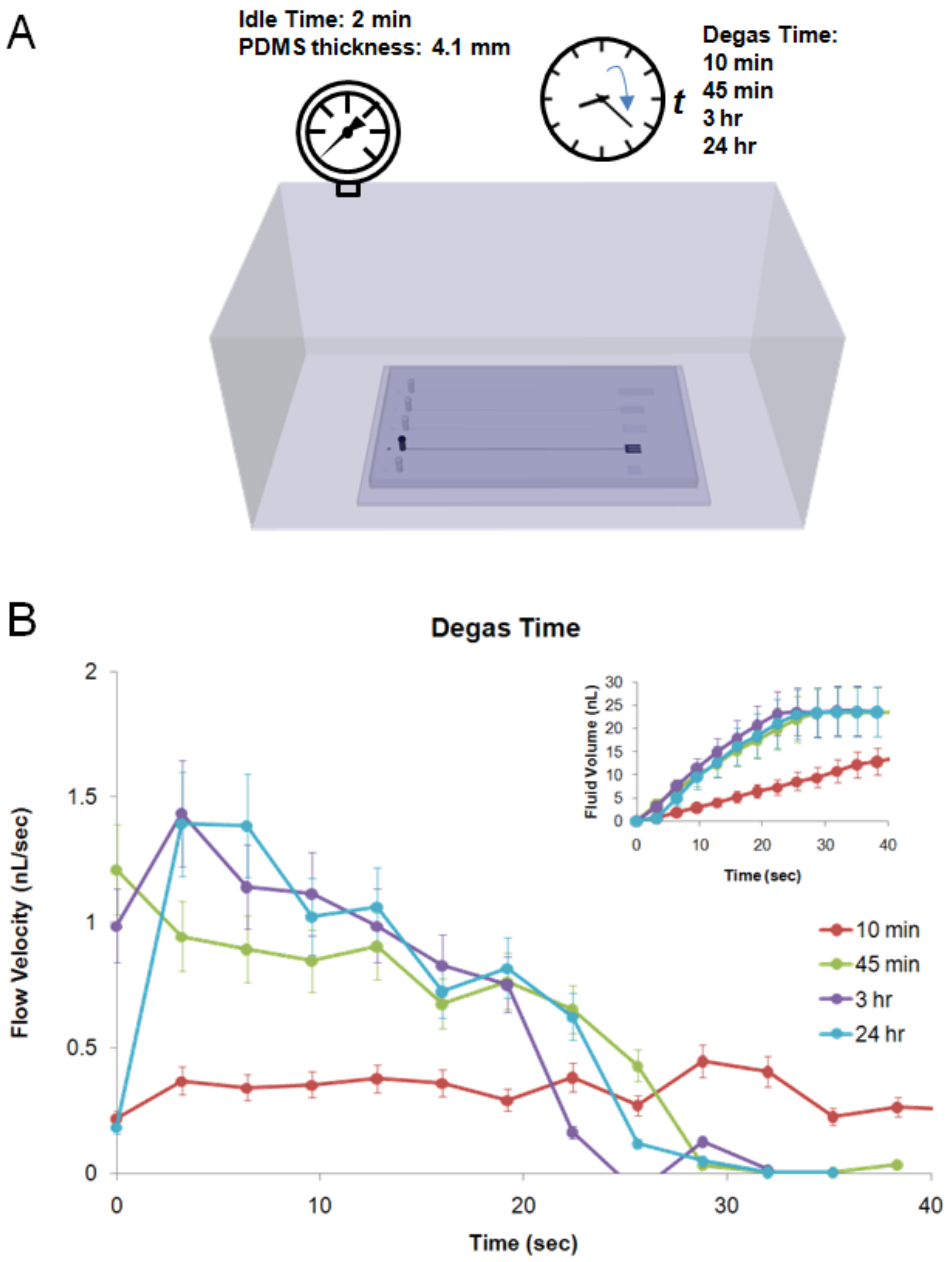

FIG 5. Effect of vacuum degas time on degas-driven flow. (A) Schematic showing device in vacuum chamber with varying degas times, ranging from 10 min to 24 hr. Data was obtained from the channel with surface area 8.85 mm^2 in Fig. 2A, with a thickness of 4.1 mm. (B) Flow velocity (main) and fluid volume profiles (inset) during channel filling for the four degas times. Error bars represent ±1.96σ of the reproducibility measurements, and the data accounts for the last 10.7 mm of the microchannel length.

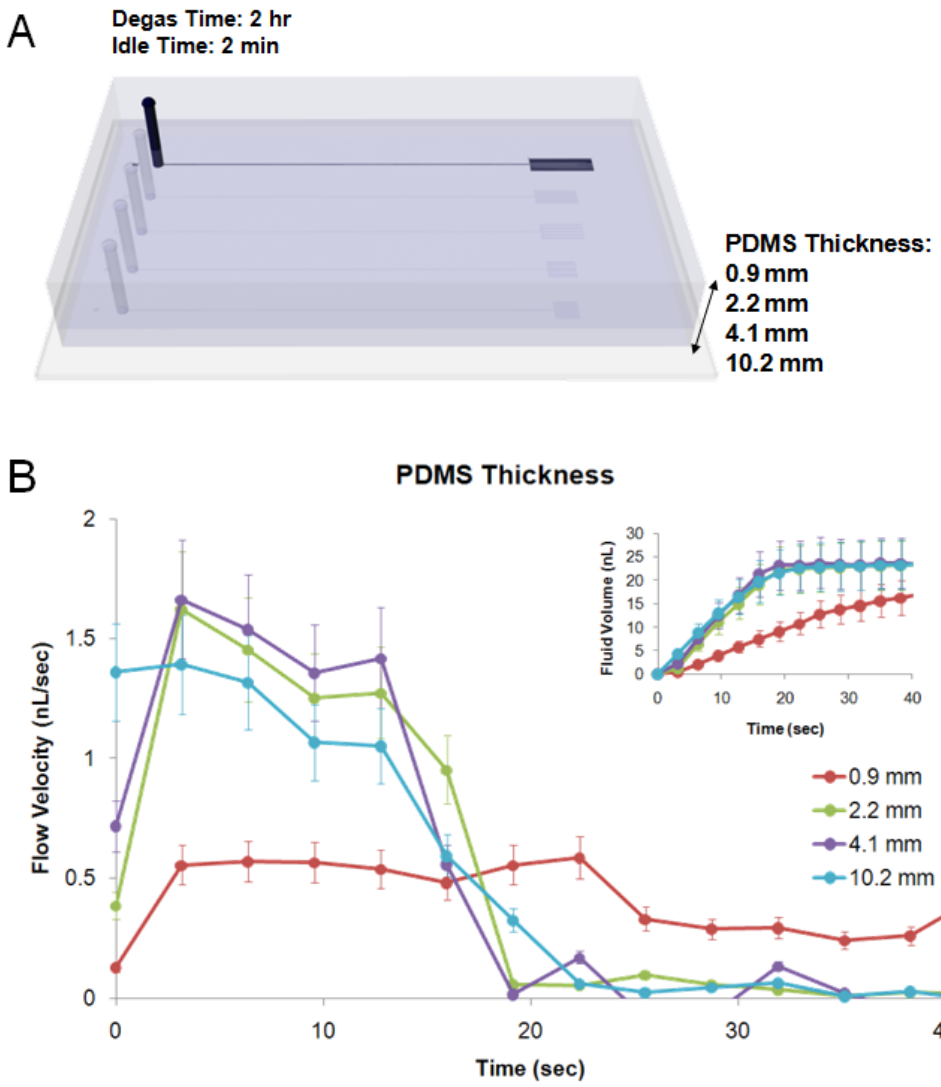

FIG 6. Effect of PDMS thickness on degas-driven flow. (A) Schematic showing device with varying PDMS thickness, ranging from 0.9 mm to 10.2 mm. Data was obtained from the channel with surface area 16.00 mm^2 in Fig. 2A, with a degas time of 2 hr and idle time of 2 min. (B) Flow velocity and fluid volume profiles (inset) during channel filling for the four PDMS thicknesses. Error bars represent ±1.96σ of the reproducibility measurements, and the data accounts for the last 10.7 mm of the microchannel length.

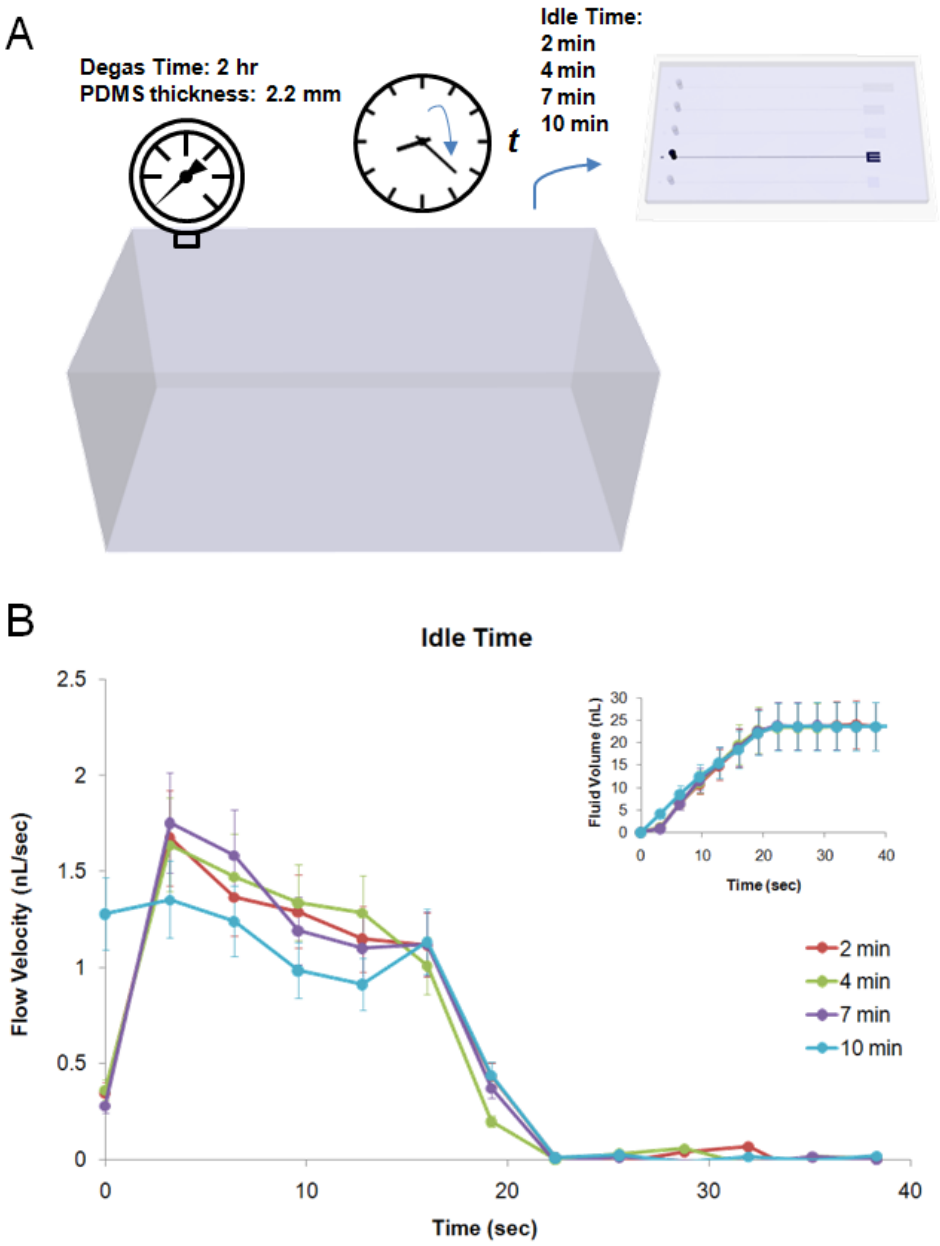

FIG 7. Effect of post-vacuum idle time on degas-driven flow. (A) Schematic showing device removed from vacuum chamber with varying post-vacuum idle times, ranging from 2 min to 10 min. Data was obtained from the channel with surface area 8.85 mm^2, with a thickness of 2.2 mm. (B) Flow velocity and fluid volume profiles (inset) during channel filling for the four post-vacuum idle durations. Error bars represent ±1.96σ of the reproducibility measurements, and the data accounts for the last 10.7 mm of the microchannel length.

A

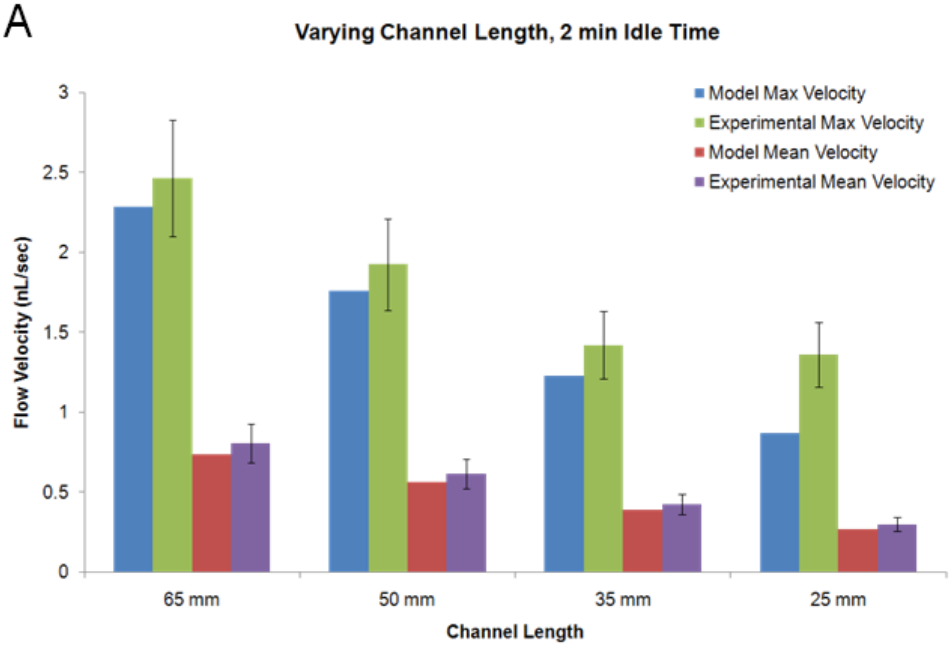
Varying Channel Length, 2 min Idle Time
Model Max Velocity
Experimental Max Velocity
Model Mean Velocity
Experimental Mean Velocity
Flow Velocity (nL/sec)
3
2.5
2
1.5
1
0.5
0
65 mm
50 mm
35 mm
25 mm
Channel Length

B

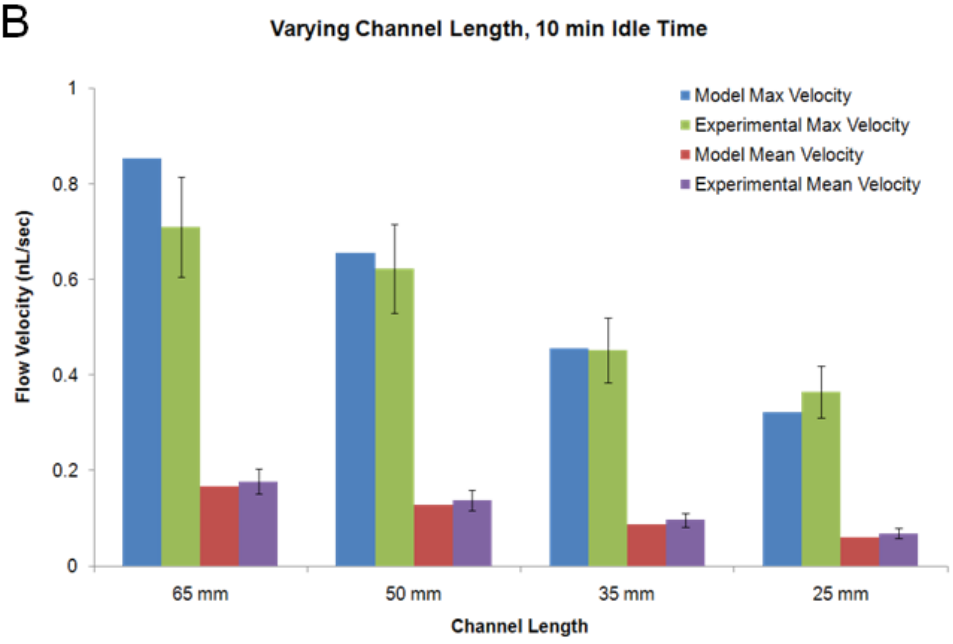
Varying Channel Length, 10 min Idle Time
Model Max Velocity
Experimental Max Velocity
Model Mean Velocity
Experimental Mean Velocity
Flow Velocity (nL/sec)
1
0.8
0.6
0.4
0.2
0
65 mm
50 mm
35 mm
25 mm
Channel Length

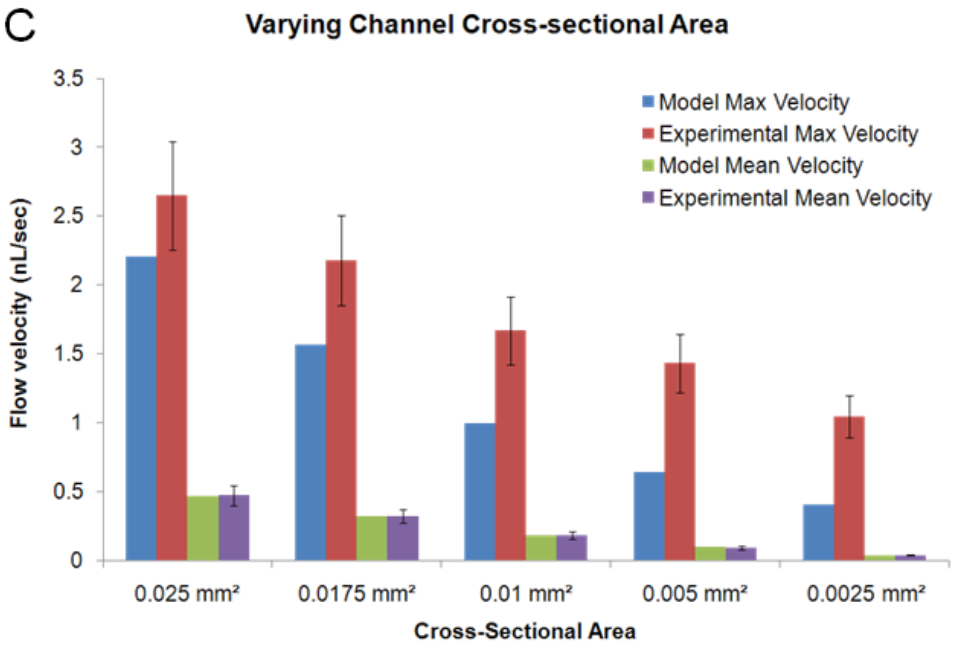

FIG 8. Effect of varying channel length, idle time, and channel cross-section on degas-driven flow. Theoretical and experimental results for maximum and mean flow velocity shown. (A) Data obtained for entire channel length for S-curve channels with lengths varying from 65 mm to 25 mm with 24 hr degas time, 2 min idle time, 4.1 mm PDMS thickness, and a 200 sec run time. (B) Data obtained for entire channel length for S-curve channels with lengths varying from 65mm to 25mm, with a 24 hr degas time, 10 min idle time, 4.1 mm PDMS thickness, and 900 sec run time. (C) Data obtained for end portion channels with cross sections varying from 0.025 mm^2 to 0.0025 mm^2, with a 24 hr degas time, 2 min idle time, 2.2 mm PDMS thickness, and a 600 sec run time. Error bars represent ±1.96σ of the reproducibility measurements.